

Research on the Tunnel Geological Radar Image Flaw Detection Based on CNN

Li He

School of Computer Science and Engineering
Xi'an Technological University
Xi'an, China
E-mail: 1003294436@qq.com

Wang Yubian

Department of Railway Transportation Control
Belarusian State University of Transport
34, Kirova street, Gomel, 246653
Republic of Belarus
E-mail: alika_wang@mail.ru

Abstract—Tunnel geological radar image has been widely used in tunnel engineering quality detection for its advantages of fast, nondestructive, continuous detection, real-time imaging, intuitive data processing and high detection accuracy. However, the traditional defect detection method, which is judged by surveyors visually, consumes energy. In order to detect the quality of tunnel engineering accurately and quickly, an improved method of void defect detection based on Faster RCNN (Regional Convolutional Neural Network) is proposed in depth learning. The image data of the tunnel geological radar is collected for annotation, which fills the blank of the defect data set in the tunnel engineering. Through the method of this paper proposed, the feature extraction is optimized to improve the performance of the detection model, and the detection accuracy of the model is verified by expert knowledge.

Keywords-Tunnel Geological; Radar Image; Flaw Detection; CNN

I. INTRODUCTION

There are a large number of tunnel projects in the construction project. The quality defects of the tunnel may affect the construction schedule, increase the engineering cost, damage the mechanical equipment and even endanger the lives of the constructor.

Geological radar detection method[1-2] is the mainstream method of tunnel lining detection at present, and has excellent performance in the detection of reinforcement and arch spacing, plain concrete structure, etc.[3]. However, the traditional survey situation is that the site construction surveyors scan the survey images generated by radar equipment one by one according to their expert knowledge. This traditional method has a large workload, a large human factor, and a certain rate of omission and error.

In recent years, with the continuous improvement of GPU, the field of deep learning is booming. In 2006, Hinton[4] and other researcher proposed the concept of deep learning, using convolutional neural network (CNN) to learn features from data. In 2012, in the ImageNet image classification competition, Alex Krizhevsky's team proposed the deep convolutional neural network AlexNet for the first time. AlexNet won the champion with an accuracy rate of 15.3% higher than the second place, which made people have a further understanding of the application of convolutional neural network in visual tasks. Girshick R proposed the regional convolutional neural network (RCNN) model, which USES the Selective Search method to select candidate regions and USES multiple

support vector machines to classify features, thus achieving target detection.

In 2015, Girshick R proposed Fast RCNN[6], which is an improved version of RCNN and adopts RoI Pooling to share the parts with a large amount of calculation to improve the working efficiency of the whole model. Later, Ren improved again on the basis of the original network, introduced RPN layer, and designed a Faster RCNN model[7], aiming at the problem that the running time of extracting candidate feature regions was slow, which achieved good results. Compared with artificially designed features, features extracted by convolutional neural network have better robustness and stronger semantic information, and great achievements have been made in computer vision fields such as face recognition[8-9], target detection, and speech recognition[10-11].

This paper selects Faster RCNN network as the basic algorithm framework for tunnel GPR (Ground Penetrating Radar) detection. The framework of Faster RCNN network is introduced. However, if the original Faster RCNN model is directly applied to the tunnel GPR detection in the actual scene, there may be two disadvantages:

1) The data sets collected on site for training are relatively small, which may lead to incomplete learning of the learning model and easy over fitting[12].

2) There are many interference factors in the tunnel, resulting in complex image features of the defect. At the same time, the radar images are all manually

experienced by field surveyors, and there is no uniform standard, so the sharpness is quite different. It will cause RPN to produce more negative sample space, and the network model is difficult to converge[13].

Based on the above reasons, this paper proposed Faster - RCNN model to expand original data sets, based on the data increase[14] and combining with GA - RPN[15] for an improvement in the target detection and evaluation index in GIoU on border regression optimization[16], in order to overcome the above shortcomings, further improve the accuracy of tunnel geological radar image detection.

II. KEY TECHNOLOGIES AND EQUIPMENT

As a relatively mature geophysical prospecting method, geological radar method has the advantages of high resolution, fast detection speed, non-destructive and radar image visualization, etc., and has become the most important method for tunnel lining quality detection. There are obvious abnormal reactions to the defects of tunnel lining, such as local un-compactness, voidage, insufficient thickness and lack of reinforcement.

A. Technical principle

Different defects have different reflections in radar images. The electromagnetic waves emitted by GPR will generate reflection and refraction on the surface of the medium with different dielectric constants[17]. The dielectric constants of common materials are shown in table 1 below.

TABLE I. DIELECTRIC CONSTANTS OF COMMON MATERIALS

Material	Dielectric constant	Velocity (mm/ns)
atmosphere	1	300
water	81	30
concrete	5-8	55-120
Sand (dry)	3-6	120-170
Sand (wet)	25-30	55-60
pitch	3-5	134-173

Reflection and refraction conform to the law of reflection and refraction. The energy of reflected wave and refracted wave depends on the reflection coefficient R and refracted coefficient T:

$$R = \frac{\sqrt{\epsilon_1} - \sqrt{\epsilon_2}}{\sqrt{\epsilon_1} + \sqrt{\epsilon_2}} \quad (1)$$

In the above equation, ϵ_1 and ϵ_2 are the relative permittivity of the upper and lower media at the interface respectively. According to Formula (1), when the electromagnetic wave propagates to the interface with dielectric constant difference, the reflected electromagnetic wave energy will change, which is reflected in the radar image as positive and anti-peak anomalies. The defects in lining such as local un-compaction, voidage, insufficient thickness and lack of reinforcement have obvious dielectric differences with concrete, which provide a good geophysical foundation for the application of GPR.

B. Equipment

The equipment of detection equipment of GPR system in the project is shown in Figure 1.



Figure 1. GPR system detection equipment

Geological ground penetrating radar method is the use of high frequency electromagnetic wave transmitting antenna will be in the form of a pulse in the concrete surface emission to concrete, the concrete interface reflection and defects return to the surface, by the receiving antenna to receive the echo signal, the treatment of radar system, radar image, through the analysis of the radar image processing, the interpretation of the data on the basis of this, so as to achieve quality nondestructive testing of lining. Its detection principle is shown in Figure 2.

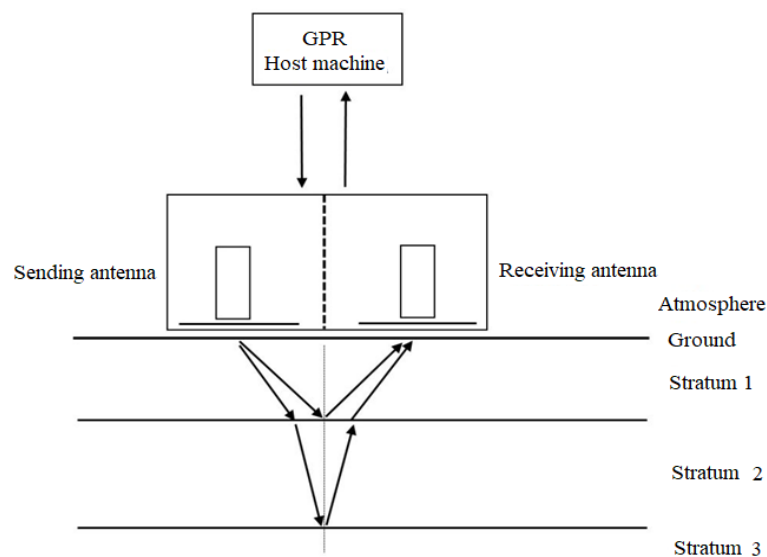


Figure 2. Principles of geological radar detection

C. The Radar imaging profile

Profiles of GPR images are usually recorded in the form of pulse reflected waves, or in the form of gray or color profiles. In this way, the in-phase axis or the iso-gray line can be used to represent the underground reflector or the target body. On the waveform recording chart, waveforms are recorded in the vertical direction of the survey line at all measurement points, forming the radar imaging profile.

In the tunnel lining detection, the voids mainly appear between the inner lining, the second lining and the surface layer. Due to the large dielectric difference between the void and surrounding media, when the electromagnetic wave propagates between concrete and atmosphere, air and surrounding rock, it will generate two strong reflections at the upper and lower interfaces.

Because the electromagnetic wave in the air attenuation is small, and the concrete and air dielectric

difference is large, so in the void to produce a strong multiple reflections, electromagnetic wave in the air medium propagation frequency is relatively high.

At the upper interface of voids, the electromagnetic wave goes from concrete to the air medium. According to the law of reflection (Formula 1), the reflection coefficient is positive, showing a negative wave peak. At the gap interface, the reflection coefficient of electromagnetic wave from air to concrete medium is negative, showing a positive wave peak. The picture is as shown in Figure 3.

In the image, white is the strongest color of positive reflection and black is the strongest color of negative reflection. In theory, there is a gap defect and the radar image shows two sets of reflected signals. In the actual survey, the second reflection signal may be lost due to signal interference.

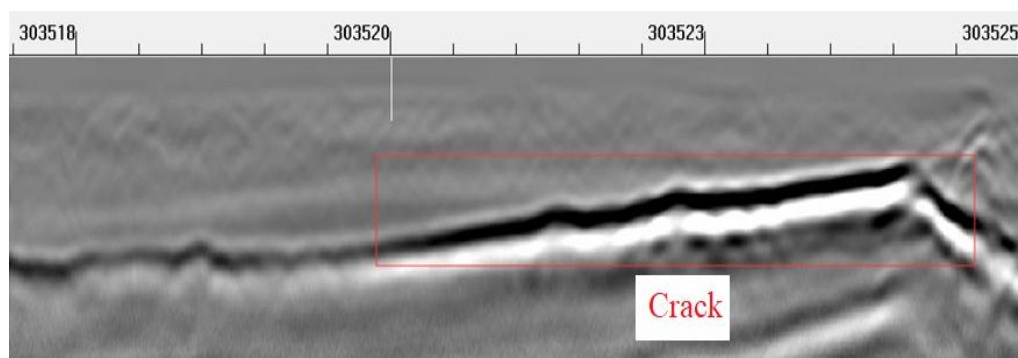


Figure 3. GPR image of tunnel ejection

III. CONVOLUTIONAL NEURAL NETWORKS

Convolutional Neural Networks (CNN) can use local operations to abstract the representations in a hierarchical way in image recognition [18]. Two key design ideas have driven the success of convolution architecture in computer vision. First, CNN USES the 2D structure of the image, and the pixels in adjacent areas are usually highly correlated. Therefore, instead of using one-to-one connections between all pixel units (as most neural networks do), CNN can use local

connections in packets. Second, the CNN architecture relies on feature sharing, so each channel (that is, the output feature graph) is generated by convolution with the same filter at all locations.

Deep learning methods of convolutional neural network are mainly divided into single-stage (eg.SDD, YOLO) and two-stage (eg.RCNN series). Single-stage generates detections directly on the picture through

calculation. Two-stage extracts the proposal first, and then makes the second amendment based on the proposal. Both are relatively single-stage fast, low precision. In this paper, it is proposed to use two-stage Faster RCNN because of the high accuracy of two-stage[19].

This paper adopts Faster RCNN as the basic framework, as shown in Figure 4. In fact, Faster RCNN can be divided into four main contents:

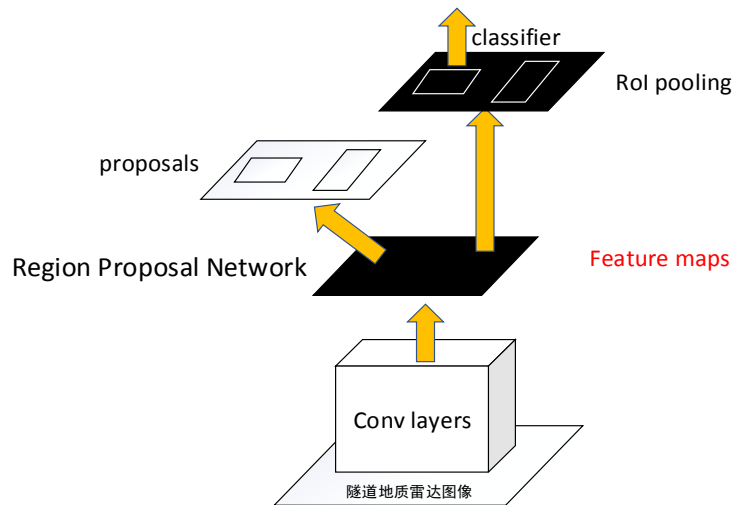


Figure 4. Structure chart Faster RCNN

1) *Convolutional layers*. It is used to extract the features of un-blemishes on the GPR image. The input is the whole image and the output is the extracted features, which are called feature maps.

2) *Region Proposal Network*. It is used to recommend candidate regions; this network is used in place of the previous search selective. The input is an image (because the RPN network and Fast RCNN share the same CNN here, so the input can also be considered feature maps), and the output is multiple candidate areas to filter out gaps in features and = perform a preliminary border regression. It shares the convolution feature of the whole graph with the

detection network, solves the speed bottleneck of the original selective search method, and greatly improves the speed of target detection.

3) *RoI pooling*. Its function is input different sizes and converted into output of fixed length, and the input and output are the same as RoI pooling in Faster RCNN.

4) *Classification and regression*. The output of this layer is the class of the fully connected neural network of candidate region, and the exact location of the candidate region in the image.

The whole process is shown in Figure 5.

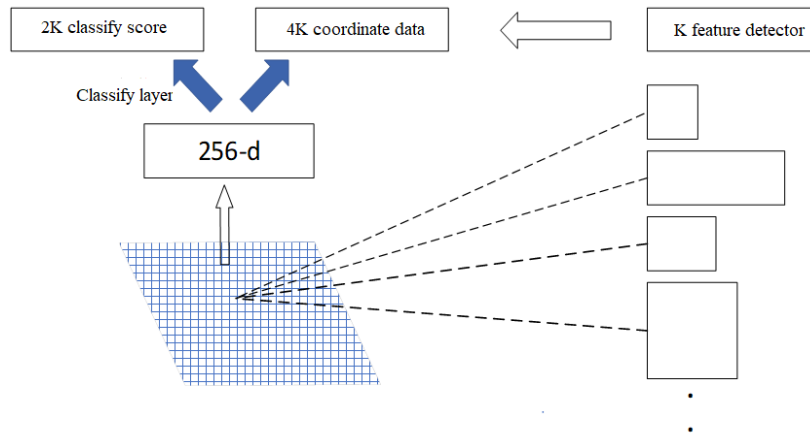


Figure 5. Structure chart of RPN

IV. GENERATING ANCHOR -RPN

Regional Anchor is an important cornerstone of target detection method at present. Most good target detection algorithms rely on the Anchors mechanism to evenly sample a given location in space with predefined sizes. There are two major problems in the process of generating Anchor by the traditional two-stage anchor-based method:

1) *Inefficient is low.* The existing method makes sliding Windows on the feature map and generates thousands of anchors. However, there are only a few objects in one picture, which leads too many negative samples.

2) *Unreasonable a priori assumptions.* When generating Anchor, it is assumed that the scale of Anchor or the length-width ratio is several fixed values. These values tend to change and change with the dataset.

According to the above Hamid Rezatofighi proposed the guided anchor in 2019. The Guided anchor mechanism works as follows: the position and shape of the target can be represented by (x, y, w, h). (x, y) represents the coordinates of the object's position in space.

If the box of the object is drawn on a given input picture, the following distribution can be obtained:

$$p(x, y, w, h | I) = p(x, y | I)p(w, h | x, y, I) \quad (2)$$

There are two important information can be obtained from the above equation: (1) the specific region of the object in the image; (2) the size and proportion of the object are closely related to its location. The anchor generated model is therefore designed to contain two branches: one for positioning and one for shape prediction.

A. Anchor generation modules.

That is position prediction module. The goal is to predict which regions should be used as the center points to generate the anchor, which is a dichotomy problem, to predict whether or not the object is the center. Two branches were added to predict the confidence of each pixel (corresponding receptive field) on the feature graph, as well as the corresponding width and height.

A target is considered a target if its confidence is greater than a specific domain value. Obviously, the process of obtaining this proposal is different from that of sliding window, which can reduce a large number of negative samples (only one proposal can be generated by making more pixels on each Feature map).

In addition, since the width and height are also regressed by CNN, there is no scale for the object, and

the width and height are compared to any prior assumptions.

B. Feature adaption modules.

This module actually quotes from the idea of deformable convolution. Firstly, the width and height of each point can be obtained by using the Anchor generation module. The width and height are represented by a 2-channel characteristic graph, and then the offset field is obtained by convolving again on the 2-channel characteristic graph. Finally, the offset field is applied to the characteristic graph.

V. IMPROVE IOU ALGORITHM

In the target detection, it depends on the regression of boundingbox coordinates to obtain accurate positioning effect. IoU (Intersection-over-Union) is an important concept in target detection. In the anchor-based method, it is not only used to determine positive samples and negative samples, but also to evaluate the distance between the predictbox and ground-truth, or the accuracy of the predictbox.

One of the better features about the IoU is that it's scale insensitive. In the regression task, the most direct indicator to judge the distance between predict box and gt is the IoU, but the loss used is not suitable. Since loss cannot reflect the regression effect, IoU can get different values according to different situations, which can most directly reflect the regression effect. But there are two problems with using IoU directly as the loss function:

- A. *If the two boxes do not intersect, by definition, IoU=0, it does not reflect the distance between them. At the same time, because loss=0, there is no gradient return, no learning and training.*
- B. *The IoU cannot accurately reflect the degree of coincidence between the two. As shown in figure 6 below, IoU is equal in all three cases, but their coincidence degree is different. The graph on the left has the best regression effect, while the graph on the right has the worst.*

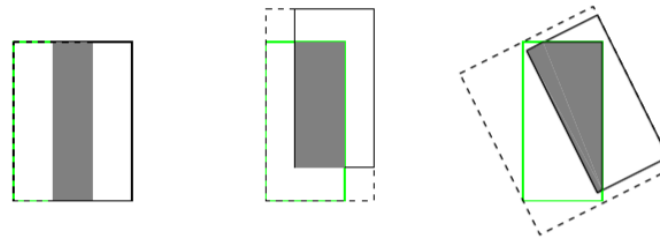


Figure 6. Same border regression of IoU

To solve the above problems, Rezatofghi, Hamid and other researcher proposed GIoU in 2019, and its algorithm formula for GIoU is as follows:

Algorithm 1: Generalized Intersection over Union

Input: Two Random image: $A, B \subseteq S \in R^n$
 Output: GIoU

1. Find the smallest target graph C that surrounds A and B, C satisfies the condition: $C \subseteq S \in R^n$
2.
$$IoU = \frac{|A \cap B|}{|A \cup B|}$$
3.
$$GIoU = IoU - \frac{|C \setminus (A \cup B)|}{|C|}$$

C. Characteristics of GIoU

1) *Similar to IoU, GIoU is also a distance measure.* As a loss function, $L_{\{GIoU\}}=1-GIoU$, which meets the basic requirements of the loss function.

2) *GIoU is Insensitive to scale.*

3) *GIoU is the lower bound on IoU, and in the case of wireless overlap between the two boxes, $IoU=GIoU$.*

4) *The value of IoU is $[0,1]$, but the value range of GIoU is symmetric $[-1,1]$.* According to the above formula, it can be seen that GIoU is always less than or equal to IoU. In addition, for IoU, its range is $[0,1]$, while the range of GIoU is $[-1,1]$. When the two shapes coincide completely, there is $GIoU=IoU=1$. When there is no overlap between the two shapes, $IoU=0$, and the subtraction is -1 .

5) *Unlike the IoU, which only focuses on the overlapping area, the GIoU not only focuses on the overlapping area, but also focuses on other non-overlapping areas, which can better reflect the coincidence degree of the two. Since GIoU introduces C containing two shapes of A and B, it can still be optimized when A and B do not coincide.*

VI. EXPERIMENTAL METHODS

A. Data to enhance

Compared with traditional images, the number of GDAR images that can provide deep learning training is generally less, and the lack of data will lead to over fitting of the model. In order to ensure the generalization ability and recognition effect of the model after training, it is more important to improve the training performance of the deep learning method by means of data augmentation. The small manually labeled data set was taken as the initial sample, and the initial sample set was rotated and compound rotated, and all the operation results obtained were taken as the training data set after data enlargement.

B. Training methods

After the data enhancement, the images of plain concrete and reinforced concrete were sent into the neural network to start the training model. Faster - RCNN model training method using alternate optimization method (alternating optimization), it is divided into four steps.

1) *Stage1_rpn_train.pt*

RPN network was trained separately, and the trained void model was initialized with the model of ImageNet, and the parameters were adjusted in an end to end manner. backbone+rpn+fast rcnn—>backbone1+rpn1+fast rcnn, backbone, rpn, parameter updating;

2) *Stage1_fast_rcnn_train.pt*

Fast RCNN is a separate training detection network. Proposals for training come from RPN net in step 1. The model initialization adopts the ImageNet model. backbone+rpn1+fast rcnn—>backbone2+rpn1+fast rcnn1, backbone, fast rcnn, parameter updating;

3) *Stage2_rpn_train.pt*

The RPN model was initialized with the parameters of the second step Fast Rcn, but the convolutional layer was fixed during the training and only the parameters belonging to RPN were adjusted. backbone2+rpn1+fast rcnn1—>backbone2+rpn2+fast rcnn1, rpn, parameter updating;

4) *Stage2_fast_rcnn_train.pt*

Keep the Shared convolutional layer fixed; fine-tune the remaining parameters of Fast rcnn with the proposals of the RPN output adjusted in step 3 as input. Backbone2+rpn2+fast rcnn1—>backbone2+rpn2 + fast rcnn2, fast rcnn, parameter updating.

The above four steps are shown in figure 7.

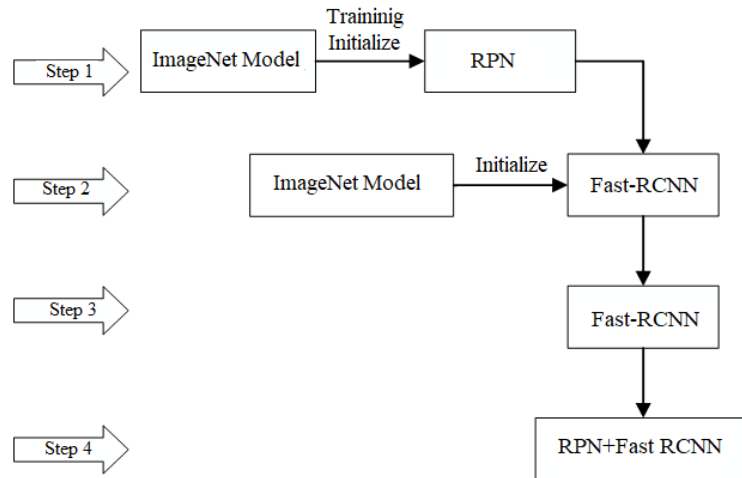


Figure 7. Network model training process

C. Evaluation index

The general formula for calculating the accuracy is: the number/total number of accurate classification $\times 100\%$ [20]. This paper uses traditional evaluation criteria

Accuracy: $ACC = (TP+TN) / (TP+TN+FP+FN)$

Precision: $P = TP / (TP+FP)$, the proportion of positive classes in the results after classification.

Recall: $RECALL = TP / (TP+FN)$, the proportion of all positive examples divided into pairs.

TP means that the positive sample is correctly identified as a positive sample.

TN means that negative samples are correctly identified as negative samples.

FP indicates that a negative sample is incorrectly identified as a positive sample.

FN means that a positive sample is incorrectly identified as a negative sample.

The identification criteria for identification of void in the tunnel lining in the image are defined as the type and location of void. The probability size and the coincidence degree of the identification box and the marker box are determined as empty. Through the analysis of the sample situation, if the probability of the

defect of the Geology radar image and the GIOU reach more than 50%, the gap will be recognized.

VII. CONCLUSION

In tunnel construction, geological radar is used to detect highway tunnel engineering, and the radar scanning result map can be used to realize advanced geological forecast, and the hidden danger of geological defects in the tunnel can be found. Based on the analysis of the elation principle, a method based on Faster RCNN is proposed in this paper to extract the position of the elation in the second lining. Compared with the traditional identification method, this method has the characteristics of Faster and higher accuracy. Since this data set is only plain concrete and reinforced concrete, the scale of annotated data will be further expanded to enrich the diversity of samples to improve the performance of the model.

REFERENCES

- [1] Li Wendi. Analysis of GPR image features of tunnel lining defects. [J]. Fujian Building Materials, 2019(01):22-24.
- [2] Zhang Chi. Research on detection of lining voids of reinforced concrete structures based on geological radar method [J]. Railway survey, 2018, 44 (03):35-38.
- [3] Liu Jinlong, Tan hailiang. Application of geological radar in detecting soil defects [J]. Engineering quality, 2018, 36 (01):73-75.
- [4] Hinton G E, Osindero S, Teh Y. A fast learning algorithm for deep belief nets [J]. Neural Computation, 2006, 18: 1527-1554.

- [5] Krizhevsky A, Sutskever I, Hinton G E. ImageNet classification with deep convolutional neural networks [J]. Communications of the Acm, 2012, 60(2): 1097-1105.
- [6] Girshick R. Fast R-CNN[C]//2015 IEEE International Conference on Computer Vision (ICCV), December 7-13, 2015, Santiago, Chile. New York: IEEE, 2015: 1440-1448.
- [7] Ren S, He K, Girshick R, et al. Faster R-CNN: towards real time object detection with region proposal networks[J]. IEEE Transactions on Pattern Analysis and Machine Intelligence, 2017, 39(6): 1137-1149.
- [8] Sun Y, Liang D, Wang X G, et al. DeepID3: face recognition with very deep neural networks [J]. Computer Science, 2015, 2(3): 1-5.
- [9] Luiz G H, Robert S, Luiz S O. Written dependent feature learning for offline signature verification using deep convolutional neural networks [J]. Pattern Recognition, 2017(70): 163-176.
- [10] Abdelhamid O, Mohamed A R, Jiang H, et al. Convolutional neural networks for speech recognition[J]. IEEE/ACM Transactions on Audio, Speech, and Language Processing, 2014, 22(10): 1533-1545.
- [11] Redmon J, Divvala S, Girshick R, et al. You only look once: unified, real-time object detection[C]//Proceedings of the IEEE Conference on Computer Vision and Pattern Recognition, June 27-30, 2016, Seattle, WA, USA. New York: IEEE, 779-788.
- [12] Du Yuhong, Dong Chao-qun, etc. Application of improved Faster RCNN model in cotton fiber identification [J/OL]. Advances in laser and optoelectronics:1-14[2019-11-25].
- [13] Xu shoukun, Wang yaru, Gu yuwan etc. Research on the detection of helmet wearing based on improved FasterRCNN [J/OL]. Computer application research: 1-6[2019-11-25].
- [14] Song Shang-ling, Yang Yang etc. Pulmonary nodules detection algorithm based on Faster-RCNN [J/OL]. Chinese journal of biomedical engineering: 1-8[2019-11-25].
- [15] Wang J, Chen K, Yang S, et al. Region Proposal by Guided Anchoring [J]. 2019. Rezaatofighi H, Tsoi N, Gwak J Y, et al. Generalized Intersection over Union: A Metric and A Loss for Bounding Box Regression [J]. 2019.
- [16] Rezaatofighi H, Tsoi N, Gwak J Y, etc. Generalized Intersection over Union: A Metric and A Loss for Bounding Box Regression[J]. 2019.
- [17] Zheng Lifei, Xiao lito, Li Xiaoqing. Forward modeling and application of geological radar advance prediction [J]. Communications science and technology, 2018(2):76-81.
- [18] Wu Zhengwen. Application of convolution neural network in image classification. Chengdu: University of Electronic Science and technology of China, 2015
- [19] Lin Gang, Wang Bo etc. Multi-target detection and positioning of power line inspection image based on improved faster-RCNN [J]. Power automation equipment, 2019, 39(05):213-218.
- [20] Sainath TN, Kingsbury B, Saon G, et al. Deep convolutional neural networks for large-scale speech tasks [J]. Neural Networks, 2015, 64:39-48.